Chapter 3. Alginate-graphene oxide hybrid gel beads: An efficient copper adsorbent material

3.1 Synopsis

Graphene has attracted tremendous research interest for its potential applications [43]. In particular, Graphene oxide (GO) acts as weak acid cation exchange resin because of the ionizable carboxyl groups, which allow ion exchange with metal cations or positively charge organic molecules [130]. Na-Alg polysaccharide polymer has potential as adsorbent material due to their biocompatibility and ability to making a gel (e.g Ca-Alg$_2$) with porous structure in the presence of divalent metal ions. This chapter is based on the favorable adsorption properties of Ca-Alg$_2$ and the properties of GO. Some researchers have explored the possibility of using polymer-GO as a bioadsorbent. However, Ca-Alg$_2$ strengthened by GO has not synthesised and applied in removing of Cu^{2+} ions from aqueous solution. The research aims to provide a new adsorbent material (Ca-Alg$_2$/GO) for the removing Cu^{2+} ions from aqueous solution.

This chapter studies the adsorption performance of calcium alginate (Ca-Alg$_2$) and Ca-Alg$_2$ with encapsulated graphene derivatives, namely graphene oxide (GO), (Ca-Alg$_2$/GO) gel beads for the successful removal of Cu^{2+} ions from aqueous solution. The synthesis and characterisation of Ca-Alg$_2$ and Ca-Alg$_2$/GO gel beads were investigated. The influence of the use of different adsorbent doses, Cu^{2+} concentrations and contact time on the adsorption process was investigated. This chapter also details the use of Langmuir isotherms and pseudo-second-order kinetic equation to investigate the equilibrium and kinetic studies of adsorption process.

This work has been published in the Journal of colloid and interface science (2013).

3.2 Introduction

Adsorption is a widely accepted technology for both organic and inorganic contaminants. It is considered as a fast and inexpensive purification method [131]. The design of adsorption processes required equilibrium adsorption data for use in kinetic and mass transfer models [132]. These models can then be used to predict the performance of the adsorption contact processes under a range of operating conditions [132]. The equilibrium isotherm plays an important role in prediction of the modelling for analysis of the data and for designing the adsorption system [132].

3.2.1 Adsorption isotherm modelling

3.2.1.1 Langmuir isotherm model

The adsorption isotherm describe the interactive relation between the adsorbate and adsorbent [133]. The Langmuir isotherm is a monolayer adsorption on a homogeneous surface where adsorption to the surface has the same activation energy with a finite number of adsorption sites [134, 135]. Langmuir isotherm assumes there is not any interaction between the adsorbed molecules [133, 134]. One of the most commonly used isotherms has been adopted in this work is Langmuir isotherm. The form of Langmuir equation can be represented by the following Equation 3.1 [136].

$$\frac{C_e}{q_e} = \frac{1}{K_L} + \frac{C_e}{q_m}$$

Equation 3.1

Where q_m is the maximum adsorption capacity (mg L^{-1}), K_L is the Langmuir affinity constant of the adsorbent with respect to the Cu^{2+} ion (L mg^{-1}). By plotting C_e/q_e versus C_e, the slope and intercept of the linear plot can be used to determine the values of q_m and K_L.

3.2.2 Adsorption kinetic modelling

The rate of adsorption process and determination of contact time required for an adsorption process can be obtained by the kinetic studies. In order to investigate the

adsorption kinetics of Cu^{2+} ion onto Ca-Alg_2 or Ca-Alg_2/GO gel beads, the pseudo-second-order model Equation 3.2 is employed to study the experimental data [136].

$$\frac{t}{q_t} = \frac{1}{K_2\, q_e^2} + \frac{t}{q_e}$$

Equation 3.2

Where K_2 (g mg^{-1} min^{-1}) is the rate constant of pseudo-second-order adsorption, q_t (mg g^{-1}) is the adsorption capacity at time t, q_e (mg g^{-1}) is the adsorption capacity at equilibrium and t (min) is the time. By plotting t/q_t versus t, the slope and intercept of the linear plot can be used to determine the values of K_2 and q_e.

The following section characterise Ca-Alg_2 and Ca-Alg_2/GO gel beads using FT-IR, TGA and FIB/SEM spectroscopies.

3.3 Synthesis and characterisation of Ca-Alg_2 and Ca-Alg_2/GO ionotropic beads

Ca-Alg_2 and Ca-Alg_2/GO ionotropic beads were fabricated using the dropping method as described by Hassan [137]. (see Chapter 2, Section's 2.4.1 and 2.4.2, respectively, for the full synthesis method). The fabricated beads were characterised by FT-IR, TGA and FIB/SEM spectroscopies. The following describes the results from each technique in detail.

3.4 Characterisation of Ca-Alg_2 and Ca-Alg_2/GO ionotropic beads

3.4.1 FT-IR spectroscopy characterisation of Ca-Alg_2 ionotropic beads

Figure 3.1 shows FT-IR spectra of (a) GO, (b) Ca-Alg_2 and (c) Ca-Alg_2/GO ionotropic beads. The spectrum of GO shows the common characteristic peaks observed in a GO sample [43]. The carboxyl groups were observed as a C=O

stretching vibration at ~ 1739 cm^{-1}, and C-O stretching vibration at ~ 1055 cm^{-1}. The peak at ~ 1624 cm^{-1} can be attributed to the presence of sp^2 network of the C=C groups. Finally, The broad peak at ~ 3414 cm^{-1} can be attributed to the presence of hydrogen bonding of the O-H groups (see Chapter 1, Figure 1.9). Figure 3.1(b) shows the FT-IR spectrum of Ca-Alg_2. The spectrum showed its characteristic peaks in agreement with the previously reported literature [133]. The spectrum shows a C-H stretching vibration at ~ 2939 cm^{-1} and C-H_2 bending at ~ 1447 cm^{-1}. An O-H stretching vibration at ~ 3445 cm^{-1} confirmed the presence of hydrogen bonding of the O-H groups. Finally, the carboxyl groups were observed as C=O stretching vibrations at ~ 1629 cm^{-1}, and C-O stretching vibrations at ~ 1045 cm^{-1}. An FT-IR spectrum of Ca-Alg_2/GO beads is displayed in Figure 3.1(c). The spectrum has a similar FT-IR spectrum of Ca-Alg_2, except of the peak at ~ 3445 cm^{-1} which corresponding to the O-H groups were shifted to smaller wavelengths (~ 3437 cm^{-1}). This can be attributed to the interaction of Na-Alg and GO through intermolecular hydrogen bonds as has been reported by He, et al. [138] and Ionita, et al. [139].

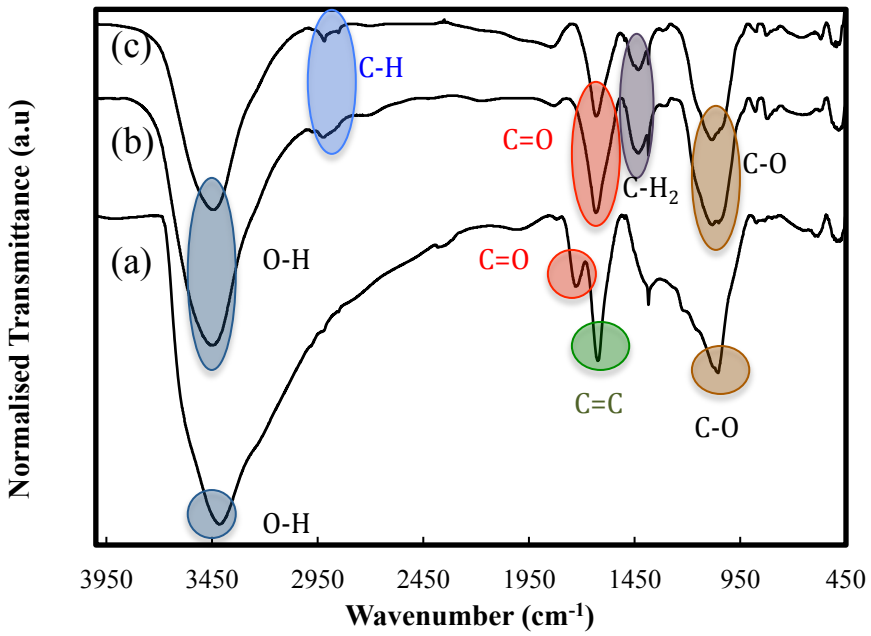

Figure 3-1 FT-IR spectrum of (a) GO, (b) Ca-Alg_2 and (c) Ca-Alg_2/GO gel beads.

3.4.2 TGA analysis of Ca-Alg$_2$ and Ca-Alg$_2$/GO beads

Ca-Alg$_2$ and Ca-Alg$_2$/GO dry beads for thermal analysis was prepared as described in Chapter 2, Section 2.7.2.1. TGA thermograms of the Ca-Alg$_2$ and Ca-Alg$_2$/GO beads are displayed in Figure 3.2. The thermogram (a) of Ca-Alg$_2$ shows three decomposition stages. The maximum decomposition (T_{max}) as well as the weight loss for each stage of the decomposition, can be found in Table 3.1. As has been explained by Zaafarany, et al. [140], the temperature of initial (T_i) and final (T_f) decomposition in the first stage was 39 and 176 °C, respectively, and the weight loss was 11.8 %. The weight loss, which observed in this stage in the TGA curve, can be explained by the dehydration of coordinated water molecules as shown in Equation 3.3:

$$C_{12}H_{14}O_{11}M.3H_2O \xrightarrow{\text{Up to 185 °C}} C_{12}H_{14}O_{11}M + 3H_2O$$

Equation 3.3

The T_i and T_f decomposition in the second stage was 176 and 389 °C, respectively, and the weight loss was 37 %. The maximum decomposition (T_{max}), which is the temperature at which maximum weight loss occurs was 222 °C. The observed weight losses, may indicate to the formation of metal oxalates intermediate fragments as shown in Equation 3.4:

$$C_{12}H_{14}O_{11}M + 10O_2 \xrightarrow{\sim 300\ °C} MC_2O_4 + 10CO_2 + 7H_2O$$

Equation 3.4

Followed by the fast third stage, the T_i and T_f decomposition in this stage was 389 and 580 °C, respectively, and the weight loss was 12 %. The weight loss in this stage may indicate to the decomposition of this metal oxalate forming the metal oxide as shown in Equation 3.5:

$$MC_2O_4 + 1/2\ O_2 \xrightarrow{\text{Up to 300 °C}} MO + 2\ CO_2$$

Equation 3.5

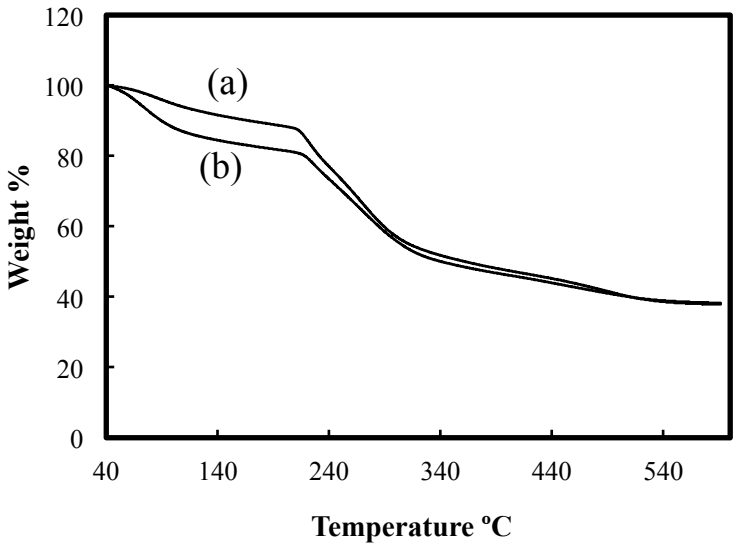

Figure 3-2 TGA thermograms of (a) Ca-Alg_2 and (b) Ca-Alg_2/GO beads.

Figure 3.2(b) shows a TGA thermogram of the Ca-Alg_2/GO beads. The TGA spectrum of GO as has been reported by [141] exhibits three stages of weight loss and this behavior is quite similar to that observed in case of Ca-Alg_2. The maximum decomposition (T_{max}) as well as the weight loss accompanying each stage of decomposition can be found in Table 3.1. It can be clearly seen that Ca-Alg_2 and Ca-Alg_2/GO differ only in the first decomposition stage. The T_i and T_f decomposition in this stage was 41 and 203 °C, respectively, and the weight loss was 18.7 %. Ca-Alg_2/GO showed much higher weight loss (~ 18.7 wt %). The weight loss observed in this stage can be interpreted as the dehydration of coordinated water molecules.

In the second stage, the T_i and T_f decomposition in this stage was 203 and 391 °C, respectively, and the weight loss was 35 %. The maximum decomposition (T_{max}) was 227 °C. The weight loss can be attributed to a decomposition of labile of oxygen

groups (carboxylic or lactone group) as well as formation of the intermediate (calcium oxalate). In the fast third stage, the T_i and T_f decomposition was 391 and 580 °C, respectively, and the weight loss was 15 % which can be explained by the decomposition of calcium oxalate as well as the removal of more stable oxygen functionalities (phenol, carbonyl, quinone).

Finally, the difference in profiles appears to indicate that the Ca-Alg_2/GO is less thermally stable than the Ca-Alg_2 with mass loss occurring at slightly lower temperatures.

Table 3-1 The maximum decomposition (T_{max}) and the weight loss accompanying to the stages decomposition.

Complexes	**Stage**	**TGA**		**Weight loss (%)**	**T_{max} °C**
		T_i °C	**T_f °C**		
Ca-Alg_2	1st	39	176	11.8	222
	2nd	176	389	37	
	3rd	389	580	12	
Ca-Alg_2/GO	1st	41	203	18.7	227
	2nd	203	391	35	
	3rd	391	580	15	

3.4.3 FIB/SEM analysis of Ca-Alg_2 and Ca-Alg_2/GO beads

Ca-Alg_2 and Ca-Alg_2/GO dry beads for FIB/SEM analysis was prepared as described

by Hassan et al [13], (see Chapter 2, Section 2.7.3.1 for full described method), which used naphthalene as a drying agent as it causes less damage to the beads than other higher temperature dehydration methods and does not cause the dried beads to shrink. FIB/SEM images of Ca-Alg_2 and Ca-Alg_2/GO beads are presented in Figure 3.3(a) and (b), respectively. It shows that there are limited porous structures in the Ca-Alg_2 (see Figure 3.3(a)) dehydrated beads. In contrast, in the case of the Ca-Alg_2/GO dehydrated beads (see Figure. 3.3(b)) more defined porous structures are observed (see Figure. 3.3(b), circled), with pore sizes ranging from 1 to 5 μ M.

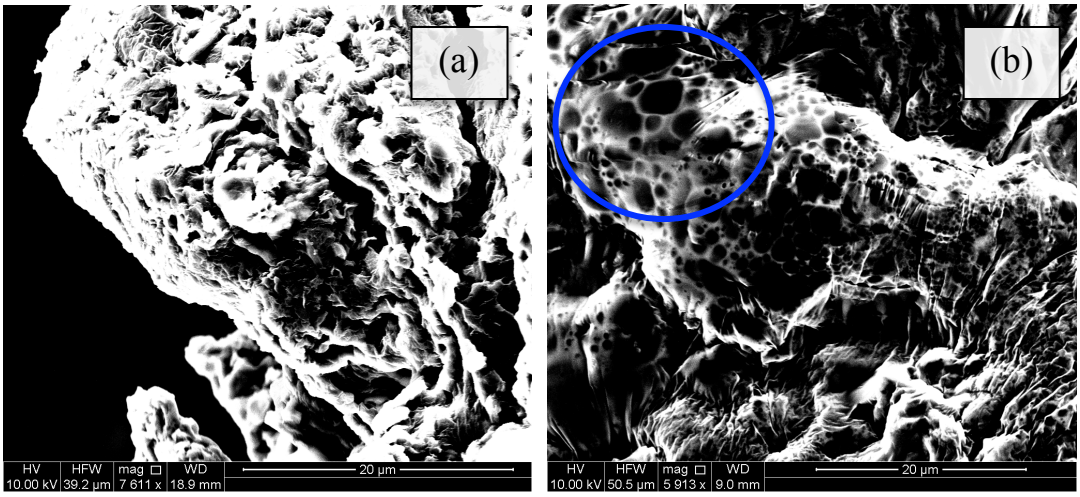

Figure 3-3 FIB/SEM images of (a) Ca-Alg_2 and (b) Ca-Alg_2/GO gel beads after drying in molten naphthalene. Circled image in (b) indicates more defined porous structure in Ca-Alg_2/GO.

3.5 Copper adsorption studies of Ca-Alg_2 and Ca-Alg_2/GO gel beads

The ability of Ca-Alg_2 and Ca-Alg_2/GO gel beads to remove copper ions from aqueous solutions was investigated in various conditions such as adsorbent doses, Cu^{2+} concentrations and contact times. The adsorption isotherms and kinetics studies were also analyzed to reveal the adsorption mechanisms. The following describes the results detail.

3.5.1 Effect of adsorbent dose (batch experiments)

Adsorbent dose is an important parameter to determine the capacity of an adsorbent for a given initial adsorbate concentration. The effect of the Ca-Alg_2 and Ca-Alg_2/GO beads dose on the remove of Cu^{2+} ion from the solution was studied. Batch experiments are done with varying the amount of Ca-Alg_2 and Ca-Alg_2/GO wet gel beads (adsorbent dose calculated at 0 g L^{-1} to 3 g L^{-1} dry weight) while the other parameters such as initial Cu^{2+} ion concentration (635 mg L^{-1}), agitation time (90 min) and volume of solution (150 mL) are kept constant. The concentration of Cu^{2+} ion in the solution was calculated from a Cu^{2+} ions calibration curve, which was developed previously from known concentration of Cu^{2+} ion (Refer to Appendices Figure 1).

The Cu^{2+} ion adsorption capacity at equilibrium (q_e) and adsorption percentage (%) was calculated according to Equation 2.1 and 2.2 (see Chapter 2, Sections 2.5.2 and 2.5.3, respectively). Figure 3.4 and Figure 3.5 display a q_e (mg g^{-1}) and adsorption percentage (%) of Cu^{2+} ions at varying adsorbent dose. From these figures, the adsorption capacity at equilibrium kept nearly constant at low adsorbent dose and decreased sharply as the dose increased. At the lowest concentration of 0.29 g L^{-1} the Ca-Alg_2 beads attained a q_e of 42.8 mg g^{-1} while the Ca-Alg_2/GO beads attained a q_e 54.9 mg g^{-1}, and at the highest concentration of 3.2 g L^{-1} the Ca-Alg_2 beads attained a q_e of 22.4 mg g^{-1} while the Ca-Alg_2/GO beads attained a q_e 26.9 mg g^{-1}. This decrease in equilibrium adsorption capacity with increasing the adsorbent doses is due to two reasons. The higher adsorbent doses provide more active adsorption sites for the Cu^{2+} ions and some remain unsaturated during the adsorption process. Secondly due to the overlapping of the adsorption sites as a result of overcrowding of adsorbent particles reduces the surface area per particle. These results suggest that a high adsorbent dose is not necessary to produce a high adsorption capacity [35, 41, 142, 143].

As can be seen from Figure 3.4 and Figure 3.5, the Cu^{2+} ion removal efficiency increased with increasing adsorbent dose for both adsorbent. At the lowest Ca-Alg_2 concentration (0.29 g L^{-1}) the percentage of Cu^{2+} ion removal from the solution were 13 % ± 0.2 and this value reached to 77 % ± 0.5 at the highest Ca-Alg_2 concentration (3.2 g L^{-1}). In contrast at the lowest Ca-Alg_2/GO concentration (0.26 g L^{-1}) the Cu^{2+}

ion removal efficiency was 15 % ± 0.6 while at the highest Ca-Alg_2/GO concentration (2.8 g L^{-1}) the Cu^{2+} ion removal efficiency increased to 81 % ±1.0. A similar result has been observed using chitosan beads, chitosan-glutaraldehyde (chitosan-GLA) beads and chitosan-alginate beads for the removal of Cu^{2+} ions from aqueous solution [142]. The results clearly show that the Cu^{2+} removal efficiency by Ca-Alg_2/GO gel beads is higher than that of Ca-Alg_2 gel beads. This can be attributed to the additional Cu^{2+} ion exchange sites within the pores of the Ca-Alg_2/GO gel beads that are available for adsorption, as observed in the SEM images (see Figure 3.3) [142, 144].

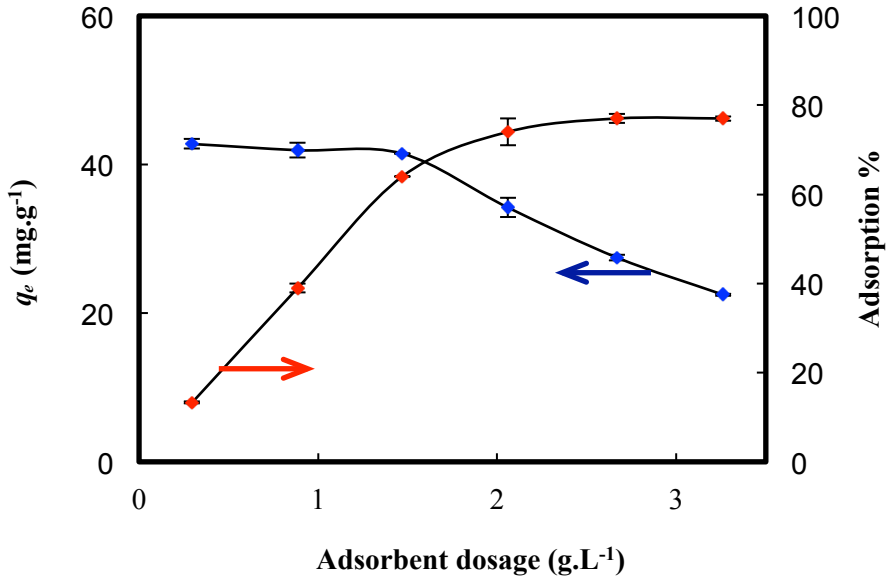

Figure 3-4 The effect of adsorbent dose on the adsorption of Cu^{2+} ions using Ca-Alg_2 (Initial Cu^{2+} ion concentration = 635 mg L^{-1}, contact time = 90 min).

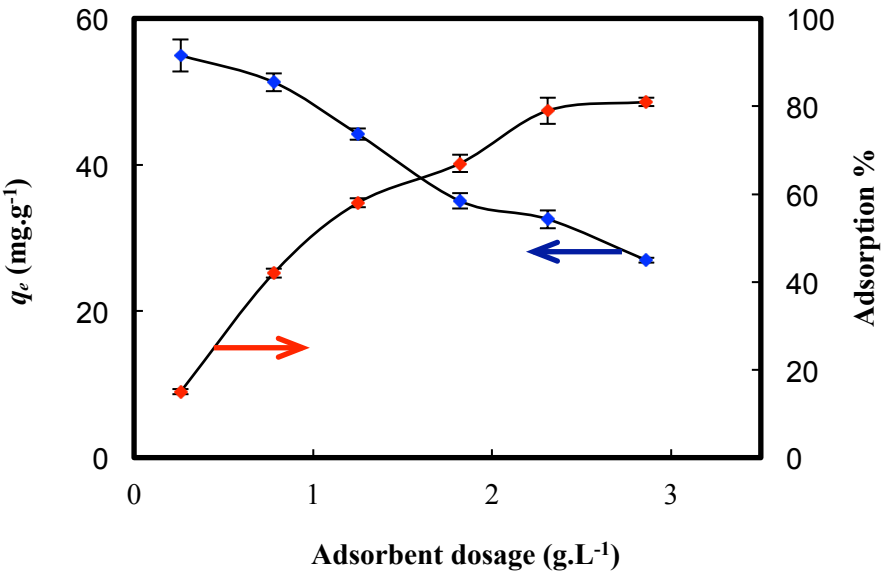

Figure 3-5 The effect of adsorbent dose on the adsorption of Cu^{2+} ions using Ca-Alg_2/GO. (Initial Cu^{2+} ion concentration = 635 mg L^{-1}, contact time = 90 min).

3.5.2 Effect of copper ion concentrations

3.5.2.1 Adsorption equilibrium isotherms

The effect of 100 gel beads from Ca-Alg_2 or Ca-Alg_2/ GO (adsorbent calculated at 0.29 g L^{-1} and 0.26 g L^{-1} dry weight, respectively) on the remove of different concentrations of Cu^{2+} ion (2.5, 5.0. 7.5, 10.0, 25.0 and 40.0 mM) from the solution was studied with a contact time of 90 min and solution volume of 150 mL. The concentration of Cu^{2+} ion in the solution was calculated as per Section 3.5.1 and the Cu^{2+} ion adsorption capacity at equilibrium (q_e) was calculated according to Equation 2.1 (see Chapter 2, Section 2.5.2). Figure 3.6 displays the adsorption isotherm data of Cu^{2+} ions adsorbed by 100 from Ca-Alg_2 or Ca-Alg_2/ GO gel beads. From this figure, it is clearly observed that the Cu^{2+} ion adsorption increases rapidly when a low initial Cu^{2+} ion concentration was used and then gradually reaches a maximum with increased Cu^{2+} ion concentration. The adsorption isotherm data in Figure 3.6 were then fitted to Langmuir isotherms (Figure 3.6, solid lines) using Equation 3.1 in Section 3.2.1.1.

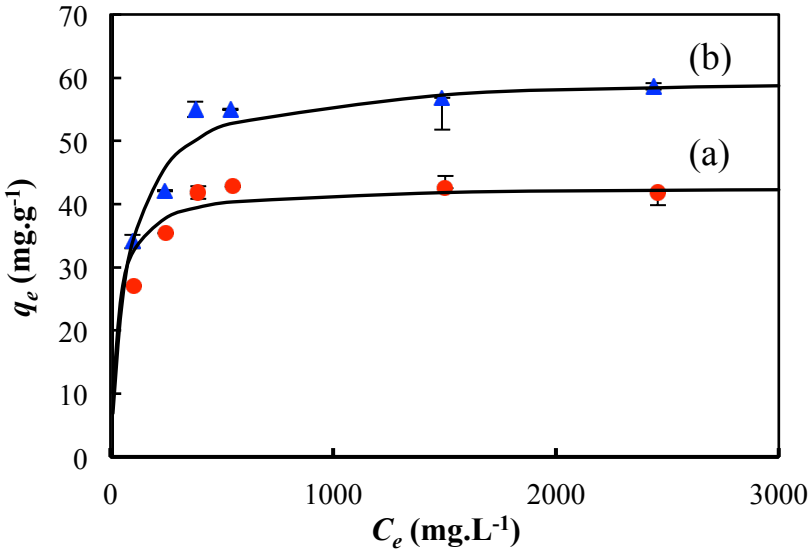

Figure 3-6 Adsorption isotherm of copper ion onto 100 beads of (a) Ca-Alg_2 with an adsorbent dose of 0.29 g L^{-1} (b) Ca-Alg_2 /GO with an adsorbent dose of 0.26 gL^{-1}, and contact time = 90 min and solution volume =150 mL. Shapes represent experimental data, while solid lines represent Langmuir modelling results.

Figure 3.7 displays the linear plots of C_e/q_e versus C_e, and q_m and K_L are determined by the slope and intercept. The values of the Langmuir isotherm constants and correlation coefficients can be found in Table 3.2. It was found that the Langmuir model exhibited a good fit to the adsorption data for Ca-Alg_2 and Ca-Alg_2/GO beads with extremely high correlation coefficients (R^2 = 0.9991, 0.9993), which indicates that the existence of homogeneous active sites on Ca-Alg_2 and Ca-Alg_2/GO beads and a monolayer adsorption behavior for Cu^{2+} adsorbed by two kinds of adsorbents beads [41, 143].

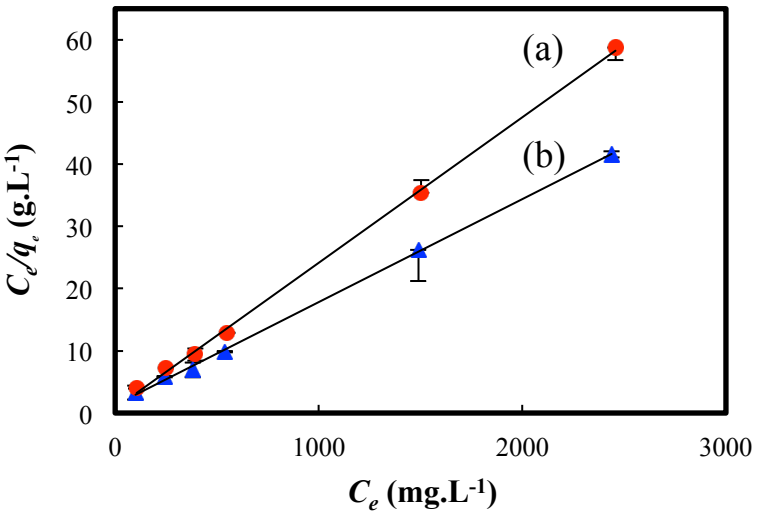

Figure 3-7 Langmuir model adsorption isotherm plot of Cu^{2+} ions adsorption onto 100 beads of (a) Ca-Alg_2 with an adsorbent dose of 0.29 g L^{-1} and (b) Ca-Alg_2/GO with an adsorbent dose of 0.26 g L^{-1}, and contact time = 90 min and solution volume = 150 mL.

The result clearly indicates that with an increase in the initial Cu^{2+} ion concentration the amount of adsorbed Cu^{2+} ions increase significantly until an equilibrium is reached corresponding to the maximum adsorption capacity q_m (42.7 and 60.2 mg g^{-1}) of Cu^{2+} ions by Ca-Alg_2 and Ca-Alg_2/GO gel beads, respectively. This due to the limited of the number of available adsorption sites as a result of a fixed amount of adsorbents beads [145]. When GO was encapsulated in the Ca-Alg_2 the q_m increased to 60.2 mg g^{-1}. This q_m value is significantly higher than for GO alone which has been shown in literature to be 46.6 mg g^{-1} [43]. Therefore there appears to be a synergistic effect by having GO within the alginate, which enhances Cu^{2+} ion maximum adsorption capacity.

Based on K_L values, which represent the affinity between the binding sites of the adsorbents and the Cu^{2+} ions, the Ca-Alg_2 gel beads show a higher affinity for Cu^{2+} ions at 0.0308 L mg^{-1} (see Table 3.2). This indicates that the Cu^{2+} ions are more easily adsorbed at the available sites on the Ca-Alg_2 beads. However, the K_L value for Ca-Alg_2/GO gel beads is lower at 0.0129 L mg^{-1} showing that it has a lower affinity for Cu^{2+} ions and indicating that the Cu^{2+} ion adsorption is at different types of

binding sites on these beads [39].

Ca-Alg_2 has two different types of binding sites, which are related to different carboxyl groups on different polymeric chains. The carboxyl groups on the homopolymeric blocks of guluronic (G-blocks) participate in an egg box structure (sol–gel transformation) in the presence of Ca^{2+} ions and are less readily available to the adsorption process. While the carboxyl groups on the mannuronic blocks (M-blocks) readily participate in the adsorption process [39]. In the case of Ca-Alg_2/GO the additional adsorption capacity of 17.5 mg g^{-1}, in comparison to the Ca-Alg_2 gel beads, may arise from the large surface area of the GO as well as other oxygen containing functional groups on the GO surface and edges participating in the chelation of Cu^{2+} ion [43].

Table 3-2 Langmuir isotherm constants and correlation coefficient of Cu^{2+} adsorption onto 100 beads of Ca-Alg_2 and Ca-Alg_2 /GO with adsorbent dose of 0.29 g L^{-1} and 0.26 g L^{-1}, respectively, contact time: 90 min and volume of solution: 150 mL.

Adsorbent	**Langmuir isotherm**		
	q_m **(mg g^{-1})**	K_L **(L mg^{-1})**	R^2
Ca-Alg_2	42.73 ± 0.37	0.0308 ± 0.01	0.9991
Ca-Alg_2/GO	60.24 ± 0.36	0.0129 ± 0.001	0.9993

3.6 Effect of contact time

3.6.1 Adsorption kinetics

The effect of contact time on Cu^{2+} ion adsorption by 100 Ca-Alg_2 and 100 Ca-Alg_2/GO wet gel beads was examined at different times from 0 to 60 min and different Cu^{2+} ion concentrations (317, 476 and 635 mg L^{-1}) (see Figure 3.8 a and b, respectively). The Cu^{2+} ion concentration was determined by the same procedure described in Section 3.5.1 and the Cu^{2+} ion adsorption capacity at time t (q_t) was calculated according to Equation 2.3 (see Chapter 2, Section 2.6). From Figure 3.8 a and b it can be seen that there is a sharp increase in the Cu^{2+} adsorption by Ca-Alg_2 and Ca-Alg_2/GO gel beads in the first 5 min for different Cu^{2+} ion concentrations.

With the further increase of contact time, the adsorption of Cu^{2+} gave a slow approach towards equilibrium until 45 min. Afterwards, no appreciable changes in the amount of adsorption were noticed. This indicates that the adsorption sites gradually became saturated as a result of increasing the contact time [143]. The adsorption capacity for the Ca-Alg_2 gel beads after 45 min is 25.7 mg g^{-1} (Figure 3.8 (a)) while for the Ca-Alg_2/GO gel beads (Figure 3.8(b)) the adsorption capacity was 18 % higher at 30.4 mg g^{-1}.

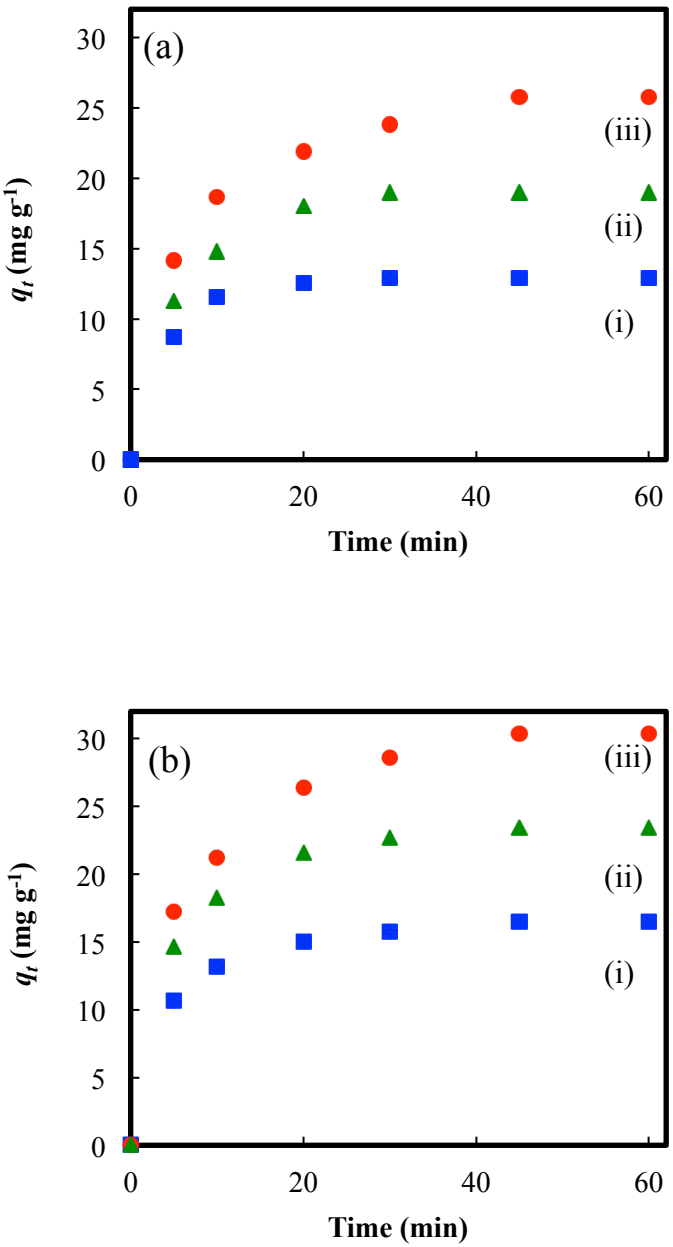

Figure 3-8 Effect of contact time on the Cu^{2+} ion adsorption of 100 gel beads (a) Ca-Alg_2 (0.29 g L^{-1} of adsorbent) (b) Ca-Alg_2/GO (0.26 g L^{-1} of adsorbent) and a solution volume = 15 mL, at a Cu^{2+} ion concentrations of (i) 317 mg L^{-1}, (ii) 476 mg L^{-1} and (iii) 635 mg L^{-1}.

In order to evaluate the adsorption kinetics of Cu^{2+} ions onto the Ca-Alg_2 and Ca-Alg_2/GO gel beads, the pseudo-second-order model (see Equation 3.2 in Section 3.2.2) is applied to analyze the experimental data as shown in Figure 3.9 a and b. The kinetic parameters and the correlation coefficients were summarized in Table 3.3. The quite high values of correlation coefficients R^2 show that the pseudo-second-

order model fit satisfactorily to the experimental data for all Cu^{2+} ion concentration onto Ca-Alg_2 and Ca-Alg_2/GO gel beads [133].

Ca-Alg_2 gel beads showed a higher kinetic rate (K_2) of 0.0425 g mg^{-1} min^{-1} than that of the Ca-Alg_2/GO gel beads at 0.0179 g mg^{-1} min^{-1}, indicating that the observed higher affinity between Cu^{2+} ions and the active sites of the Ca-Alg_2 gel beads results in faster adsorption of Cu^{2+} ions. The higher kinetic rates observed for the Ca-Alg_2 beads can be explained by the uniform availability of Cu^{2+} ion binding sites from outside to inside of the gel beads, which can be saturated quickly with Cu^{2+} ions [146]. Whereas for the Ca-Alg_2/GO beads the slower adsorption kinetics may be a result of the hybrid porous structure and the presence of the GO nanosheets in the structure may hinder the penetration of Cu^{2+} ions on the outside of the gel bead surface. However, the adsorption capacity of the Ca-Alg_2/GO beads (between 17.45 and 33.22 mg g^{-1}) was higher than that of Ca-Alg_2 beads (between 13.36 and 28.16 mg g^{-1}), indicating that the larger surface area of GO and oxygen containing functional groups on the GO surface places a strong role in increasing the adsorption capacity [43].

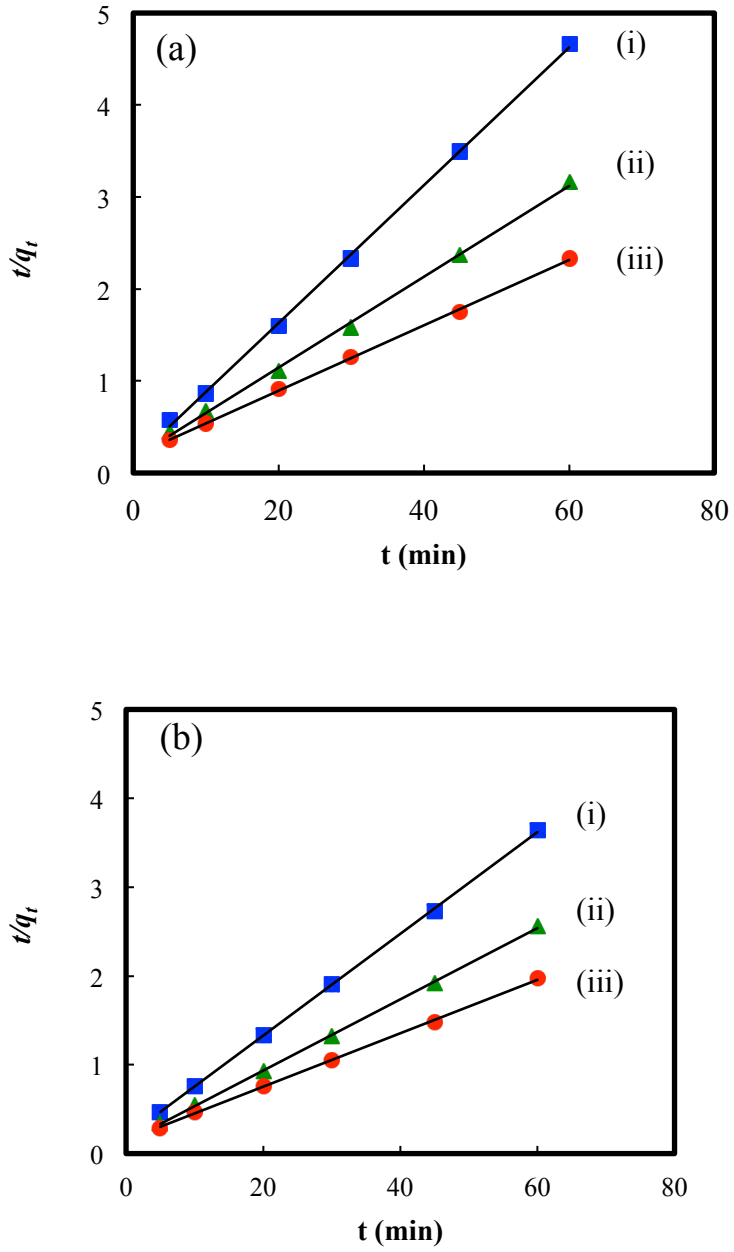

Figure 3-9 Pseudo-second-order kinetic plots for the adsorption of Cu^{2+} ions on (a) Ca-Alg_2 (0.29 g L^{-1} of adsorbent) and (b) Ca-Alg_2/GO (0.26 g L^{-1} of adsorbent) gel beads and a solution volume = 15 mL, at a Cu^{2+} ion concentrations of (i) 317 mg L^{-1}, (ii) 476 mg L^{-1} and (iii) 635 mg L^{-1}. Lines represent the fitting data to equation 3.2.

Table 3-3 The equilibrium adsorption capacity (q_e), the rate constant (K_2) and the correlation coefficients (R^2) of the pseudo-second-order kinetic for Cu^{2+} ion adsorption onto Ca-Alg_2 and Ca-Alg_2/GO gel beads.

Adsorbent	**Concentration of Cu^{2+} ion solution (mg L^{-1})**								
	317			**476**			**635**		
	q_e (mg g^{-1})	K_2 (g mg^{-1} min^{-1}	R^2	q_e (mg g^{-1})	K_2 (g mg^{-1} min^{-1}	R^2	q_e (mg g^{-1})	K_2 (g mg^{-1} min^{-1}	R^2
Ca-Alg_2	13.36	0.0425	0.9992	20.24	0.0150	0.9984	28.16	0.0068	0.9993
Ca-Alg_2/GO	17.45	0.0179	0.9998	24.93	0.0121	0.9996	33.22	0.0059	0.9993

3.7 Concluding remarks

This chapter investigated the adsorption performance of Ca-Alg_2 and Ca-Alg_2/GO gel bead adsorbents for the removal of Cu^{2+} ions from aqueous solution. Ca-Alg_2 and Ca-Alg_2/GO gel beads were synthesised by dropping method. The adsorbents were characterised using FT-IR, TGA and FIB/SEM. FT-IR spectroscopy confirmed that the Ca-Alg_2 and Ca-Alg_2/GO gel beads were produced. TGA analysis showed that Ca-Alg_2/GO gel beads is less thermally stable than the Ca-Alg_2 gel beads, and this may be attributed to enhanced thermal conductivity of GO aiding bond cleavage. FIB/SEM images of the adsorbents showed that the limited porous structures in the Ca-Alg_2 dehydrated beads, whereas, in the case of Ca-Alg_2/GO dehydrated beads more defined porous structures was observed with pore size ranging from 1 to 5 μM.

Cu^{2+} adsorption studies were conducted by considering the influence of different adsorbent doses, Cu^{2+} concentrations and agitation periods. It was found that q_e was reduced from 42.8 to 22.4 mg g^{-1} and from 54.9 to 26.9 mg g^{-1} for Ca-Alg_2 and Ca-Alg_2/GO gel beads, respectively, with increasing the adsorbent dose at the same concentration of Cu^{2+} ion solution. This can be attributed to that the higher adsorbent doses provide more active adsorption sites for the Cu^{2+} ions and remain unsaturated during the adsorption process. Furthermore, the overlapping of the adsorption sites as a result of overcrowding of adsorbent particles reduces the surface area per particle. In contrast, the removal efficiency of Cu^{2+} ions were increased from 13 to 77 % and from 15 to 81 % by Ca-Alg_2 and Ca-Alg_2/GO gel beads, respectively, with increasing adsorbent dose. The results showed that the Cu^{2+} removal efficiency by Ca-Alg_2/GO gel beads was higher than that of Ca-Alg_2 gel beads, which can be explained by the difference in the adsorption sites between Ca-Alg_2 and Ca-Alg_2/GO gel beads.

The effect of using different Cu^{2+} concentrations on the adsorption process also investigated. It was found that the affinity between the Ca-Alg_2 and the Cu^{2+} ions was higher than the Ca-Alg_2/GO, which represented from K_L values. It was found that the q_m increased from 42.7 to 60.2 mg g^{-1} for Cu^{2+} ion by Ca-Alg_2 and Ca-Alg_2/GO gel beads, respectively. This difference can be attributed to the large surface area of the

GO as well as other oxygen containing functional groups on the GO surface and edges participating in the chelation of Cu^{2+} ion.

Additionally, the effect of contact time on Cu^{2+} ion adsorption by Ca-Alg_2 and Ca-Alg_2/GO gel beads was investigated. The pseudo-second-order was applied to analyze the data. Ca-Alg_2 gel beads showed a higher K_2 of 0.0425 g mg^{-1} min^{-1} than that of the Ca-Alg_2/GO gel beads at 0.0179 g mg^{-1} min^{-1}. This can be explained by the uniform availability of Cu^{2+} ion binding sites from outside to inside of the gel beads, which can be saturated quickly with Cu^{2+} ions in the case of Ca-Alg_2 gel beads. Whereas for the Ca-Alg_2/GO beads the slower adsorption kinetics may be a result of the hybrid porous structure and the presence of the GO nanosheets in the structure may hinder the penetration of Cu^{2+} ions on the outside of the gel bead surface.

However, the q_e of the Ca-Alg_2/GO beads (between 17.45 and 33.22 mg g^{-1}) was higher than that of Ca-Alg_2 beads (between 13.36 and 28.16 mg g^{-1}), indicating that the larger surface area of GO and oxygen containing functional groups on the GO surface places a strong role in increasing the adsorption capacity.

Ca-Alg_2 importance is not limited to water treatment but it is also one of the most candidates for a delivery matrix. The release of three molecules namely rose Bengal (RB), Rubpy and camptothecin (CPT) from Ca-Alg_2 was investigated in the following chapter (Chapter 4). The influence of using different pH of the release media also studied. Additionally, Modification of Na-Alg by grafting with β – cyclodextrin (β-CD) was synthesised, and characterised. This was investigated in Chapter 5.